Viscosity and Rheological Behavior of Microbubbles in Capillary Tubes

Mohammad Mehdi Shams
Schulich School of Engineering, Dept. of Chemical and Petroleum Engineering, University of Calgary, Calgary, Alberta, Canada, T2N 1N4

Mingzhe Dong
Schulich School of Engineering, Dept. of Chemical and Petroleum Engineering, University of Calgary, Calgary, Alberta, Canada, T2N 1N4

College of Petroleum Engineering, China University of Petroleum (Huadong), Qingdao, Shandong, China

Nader Mahinpey
Schulich School of Engineering, Dept. of Chemical and Petroleum Engineering, University of Calgary, Calgary, Alberta, Canada, T2N 1N4

DOI 10.1002/aic.14434
Published online March 17, 2014 in Wiley Online Library (wileyonlinelibrary.com)

The viscosity of microbubbles has been measured in capillary tubes. Experiments were conducted in tubes of different diameters and lengths, with a constant microbubble concentration. The effects of bubble void fraction and size distribution on the viscosity of microbubbles were also investigated. Microbubbles demonstrate shear-thinning non-Newtonian behavior. The viscosity of microbubbles decreases with a decrease in tube diameter and bubble void fraction, and with an increase in tube length. Although viscosity changes with tube dimensions, the flow index (n') is only influenced by the microbubble void fraction. It is also found that bubble size distribution in the range (1–12 μm) used in this study does not affect the viscosity of microbubbles. The data were then used to develop a correlation to predict viscosity of microbubbles, which represents the experimental viscosity data with an absolute average relative deviation less than 1.3%. © 2014 American Institute of Chemical Engineers *AIChE J*, 60: 2660–2669, 2014
Keywords: microbubbles, capillary tube, rheology, viscosity

Introduction

Recently, microbubbles have received a great deal of attention in various fields, due to their special properties. First invented by Sebba,[1] these bubbles in liquids were stable with a shell created by surface active agents. Microbubbles are called colloidal gas aphrons (CGA) due to their surface properties.[2]

The special structure and stability of microbubbles have made them suitable for many applications. Their small size increases the active surface area required to adsorb contaminants in microflotation purposes.[3] Stability under pressure and the ability to act as contrast agents against ultrasound waves have made microbubbles an appropriate candidate for drug delivery and *in vivo* ultrasonic imaging.[4] Their stability under pressure also results in a sealing ability, which is utilized in drilling muds to reduce mud loss in high permeability reservoirs.[5] Beside their stability, the increase in viscosity due to their presence in aqueous solutions can result in an increased sweep efficiency, which has been exploited in waterflooding enhanced oil recovery instead of polymer injection.[6] Another possible application is CO_2 sequestration for greenhouse gas reduction by underground injection. In this type of injection, the stability and small size of microbubbles are used to provide a leak-free injection with higher dissolution in saline aquifers.[7,8] It has also been reported that, in some reservoirs, the gas derived from oil due to a decrease in pressure, will form microbubbles instead of conventional large bubbles. These microbubbles have been found to preserve the pressure inside of the reservoir and, thus, increase oil recovery. This form of microbubbles in oil is called foamy oil.[9] Most of the applications mentioned, involve microbubble flows in capillary environments; therefore, it is important to have a complete understanding of their behavior in capillary flows.

There have been numerous investigations on the effect of bubbles on wall friction and on bubble distribution in the cross section of the flow.[10–16] However, most of these studies focus on either large bubble sizes (0.5–2 mm) or flows in vertical tubes. It has been indicated by several investigators that the presence of bubbles results in a flattened liquid velocity at the center of the tube.[10–13] This behavior is caused by the bubble void fraction distribution along the cross section. It is shown that bubble distribution reaches its maximum close to tube wall. This maximum is more pronounced as the continuous phase Reynolds number

Correspondence concerning this article should be addressed to M. Dong at mingzhe.dong@ucalgary.ca.

$\left(Re_c = \frac{\rho_c VD}{\mu_c}\right)$ reaches values under 5000 ($Re_c < 5000$). In the case of higher Re_c values, the suspensions behave as a homogenous flow.[14] These investigators have also demonstrated that, as the bubble size decreases, the bubbles tend to migrate closer to tube walls. Presence of bubbles close to tube walls result in an increased friction to the flow.

All of these studies have focused on bubble size in range of 0.5–2 mm. Therefore, investigations conducted in horizontal tubes have resulted in a partial separation of bubbles from the flow. The separation has caused a denser collection of bubbles on the top part of the tube.[15] This behavior has been more pronounced in the case of low Re_c values. There have also been investigations done on microbubbles in horizontal tubes. Chernyshev[16] investigated microbubble (mean diameter = 40 μm) behaviors in tubes; the effect of microbubbles on the wall friction factor in tubes with diameters of 1.8 and 2.9 cm was considered. It was found that the increase in wall friction factor was only a factor of the Re_c and the bubble void fraction. Besides, Tseng et al. have conducted experiments on microbubble flow through rectangular horizontal tubes.[17] In their study, they measured both effective viscosity and friction factor of microbubbles. However, their study was focused on high bubble void fractions (71–64%) of microbubbles in high shear rates (1000–7000 s^{-1}). To our knowledge, investigations have not yet been conducted to relate the viscosity of microbubbles to the wall friction factor in very small Re_c ($Re_c < 50$) in capillary tubes. Moreover, the viscosity of microbubble suspensions in capillary environments is one of the most important parameters involved in understanding their behavior.

In this study, the viscosity of microbubbles is measured in capillary tubes using a pressure drop along the tubes. The effect of tube diameter, tube length, microbubble void fraction, microbubble size distribution, and the Re_c on the rheological properties of microbubbles is taken into consideration. Subsequently, the experimental data have been used to develop a correlation to predict viscosity in capillary tubes. The rest of this article is organized as follows: first, we present the experimental section describing the method, materials, and procedure; afterward, rheology of microbubbles is described; then a correlation to regenerate the experimental viscosity data is presented; finally comes the results and discussion section, followed by conclusions.

Experimental

Microbubble generator

Microbubble generators trap gas into a liquid using jet entrainment, cavitation, or turbulence at the gas–liquid interface to entrain bubbles into the liquid. Common methods of microbubble generation are ultrasound cavitation,[18,19] coaxial electrohydrodynamic atomization,[20] microfluidic T-junction,[21–23] and a high-speed mixer.[24,25] Although some methods are capable of generating more uniform bubbles, others are easier to operate and are used for bulk production of microbubbles. In this study, the apparatus introduced by Sebba[24] was used with some modifications, as shown in Figure 1. The main part of the generator is the impeller, which is surrounded by a perforated casing and functions as the baffles. Air bubbles entrain into the water when agitations created by the impeller move through the perforations. The spinning impeller was mounted 5 cm below the liquid surface. The speed of the impeller was found to have an impact

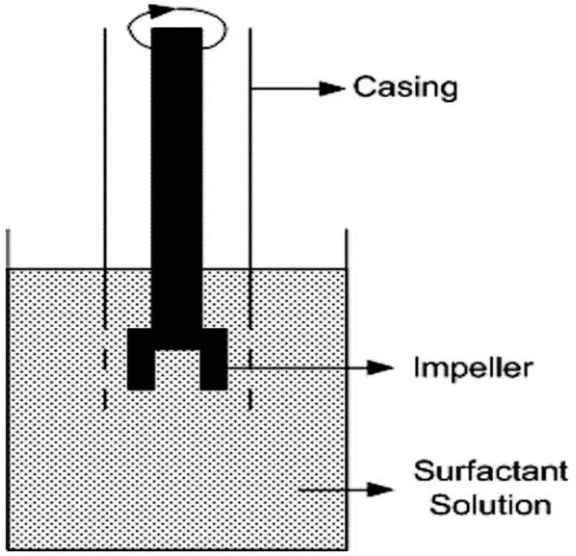

Figure 1. Microbubble generator (modified high speed mixer based on Sebba[24]).

on microbubble size distribution and stability. At low spinning speeds, the generated bubbles showed low stability. Conversely, high spinning speeds created very small bubbles not suitable for microstudies. In this work, 13,000 rpm was the optimum spinning speed, generating the optimum bubble size with a good stability.

As mentioned by Save and Pangarkar,[26] spinning times below a certain value could affect the stability of the generated bubbles. The effect of spinning time was investigated to find the threshold after which the time of spinning did not affect the stability of bubbles. It was found that 5 min of mixing would generate bubbles with good stability. Mixing times of more than 5 min have not shown an improvement on stability. The bubbles were found to remain stable for 12 h, which was adequate to complete a series of experiments.

Materials

In this study, air was used as the gas phase and a mixture of hydrophobic and a hydrophilic surfactant in deionized (DI) water was used as the liquid phase. The reason to select air as the gas phase is twofold: first, because of the ease of access to air and, second, to minimize gas phase solubility in the liquid phase.

Single surfactant solutions have been reported to either not be capable of generating bubbles or generating bubbles with short life spans.[25] Conversely, combinations of hydrophobic and hydrophilic surfactants have been reported to generate stable microbubbles.[27,28] Microbubbles produced with this kind of mixture are surrounded by a trilayer of surfactants. The hydrophobic surfactant creates a viscous layer around the bubble. The hydrophilic surfactant is present in an inner layer between gas phase and the viscous layer. Because the outer boundary of the viscous layer should be in contact with water phase, another layer of hydrophilic surfactant is also required to cover the interface of the viscous layer and water. Surfactant molecules in this layer are hydrophilic inward and hydrophobic outward; therefore, for the bubble to be in contact with water, another layer of hydrophilic surfactant is required to be hydrophobic inside and hydrophilic outside (Figure 2).[2]

A mixture of 1 g/L sorbitan monostearate (Span 60) and 1 g/L sodium dodecyl sulfate was used to include the

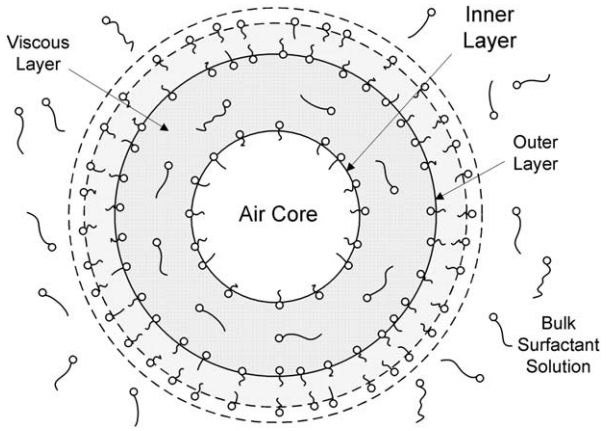

Figure 2. Structure of CGA.[2]

hydrophobic and hydrophilic surfactants, respectively. This concentration of both surfactants has been reported by Wan et al.[25] to form the most stable microbubbles. To create stable microbubbles, both of the surfactants need to be dissolved in water. As Span 60 is a hydrophobic surfactant, it hardly dissolves in water. For its complete dissolution in water, it was necessary to leave the mixture for 24 h to let the Span 60 adsorb water. The surface tension of the mixture was obtained by the pendant drop method and determined to be 44.3 mN/m. Moreover, the viscosity of the mixture was measured to be constant 0.99 mPa s at different shear rates. The density of the mixture was found to be equal to 1.03 g/cm^3.

Microbubble flow test setup

A schematic diagram of the setup used in the experiments is shown in Figure 3. The main element of the setup is a circular glass tube (PYREX Brand Glass Tubing). Tube diameters of 0.47, 1.04, and 1.37 mm were used. As tube diameter has an extensive effect on calculations, the tube diameters were measured by taking pictures of a cross section of the tubes by a microscope (Scioptic LTM-402) with a maximum magnification power of 1000X. Tube lengths of 0.75, 1.00, and 1.22 m were used to see the effect of tube length.

Both ends of the glass tube were connected to three way plexiglass chambers. The injection chamber was connected to the injection lining, transducer, and the tube. The effluent chamber was connected to the effluent lining, transducer, and the tube. During pressure measurements, it was confirmed that there was no air trapped in the chambers in order to prevent errors. In the lining connecting the glass tube to the transducer, several valves were used. The purpose of the valves was twofold: first, to protect the transducer from over range pressures and, second, to calibrate the transducer (which will be explained more later).

The injection of the microbubbles into the capillary tube was carried out by a pulse-free constant flow syringe pump (Teledyne ISCO 500D). The microbubble suspension was first transferred to a transfer cylinder and then injected from

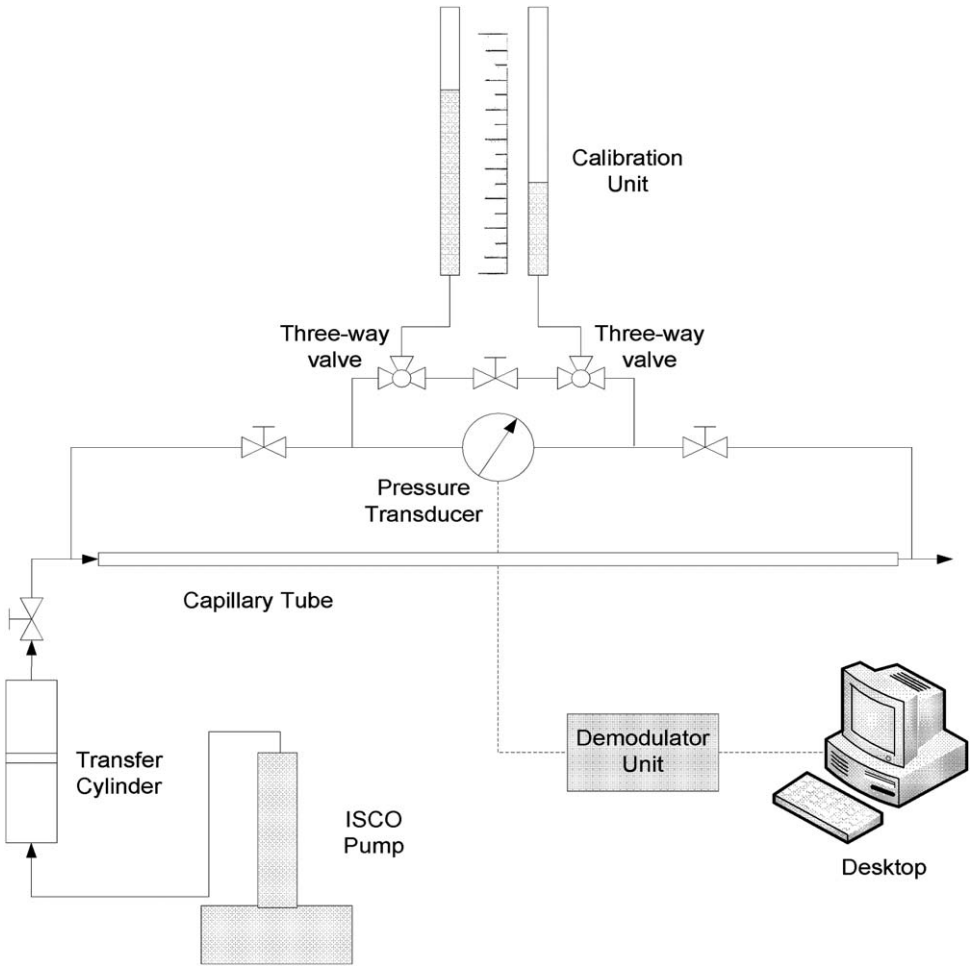

Figure 3. Schematic diagram of capillary tube setup.

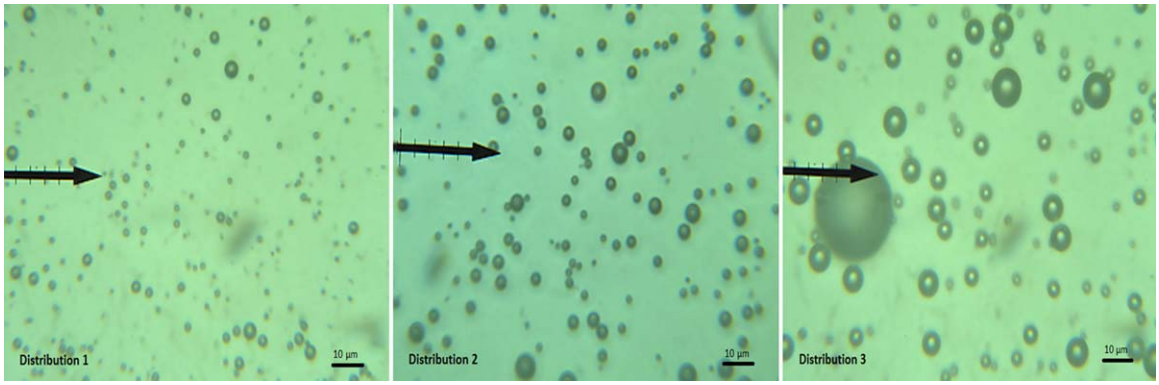

Figure 4. Photos of microbubbles with three different bubble size distributions.

[Color figure can be viewed in the online issue, which is available at wileyonlinelibrary.com.]

the transfer cylinder at an accurate constant flow rate using the syringe pump. Before the injection of the microbubble suspension, DI water was circulated through the setup to fill the teflon tubes with water, to eliminate the presence of microbubbles in the connection lines, the presence of which may affect the pressure measurement.

Procedure

To measure the viscosity of the microbubble suspension through the capillary tube, the differential pressure was measured using a high-sensitive pressure transducer, DP103 (Validyne Engineering). Electric signals transmitted by the transducer were switched to digital signals by a demodulator (Validyne CD15) so as to be readable by the computer software (Instacal Version 5.52). For the comprehension of the signals, the transducer should first be calibrated using water column. Calibration was performed by reading the signals at three different water column heights. The line connecting these three points provided the equation to convert signals to differential pressures.

Before each flow test, microphotographs of the generated microbubbles were taken using a microscope (Scioptic LTM-402) with a maximum magnification power of 1000X. The size distribution and void fraction of microbubbles for each flow test were analyzed. Because the bubble void fraction is expected to have an important role in microbubbles' flow behavior, microphotographs of the initial and effluent microbubbles in each test were taken and analyzed to assure the constant void fraction of microbubbles through the capillary tubes. Microphotographs and size distribution for three different bubble size distributions are shown in Figures 4 and 5, respectively.

Pressure drops of microbubble suspensions were measured for different tube diameters, tube lengths, flow rates, and gas void fractions. All of the pressure drop measurements were conducted at a constant temperature (21°C). The effect of each parameter was investigated by keeping the other variables constant. Beside using the aforementioned tube diameters and tube lengths, four gas void fractions of 3.4, 4.9, 6.4, and 7.8% were used to study the effect of gas percentage on the viscosity of microbubble suspensions. Furthermore, to examine the dependence of viscosity on flow rate, the pressure drop was measured in different flow rates while keeping the other variables constant. Because the effect of flow rate was investigated through Re_c, flow rates examined were carefully chosen to yield equal Re_c numbers in different tube diameters.

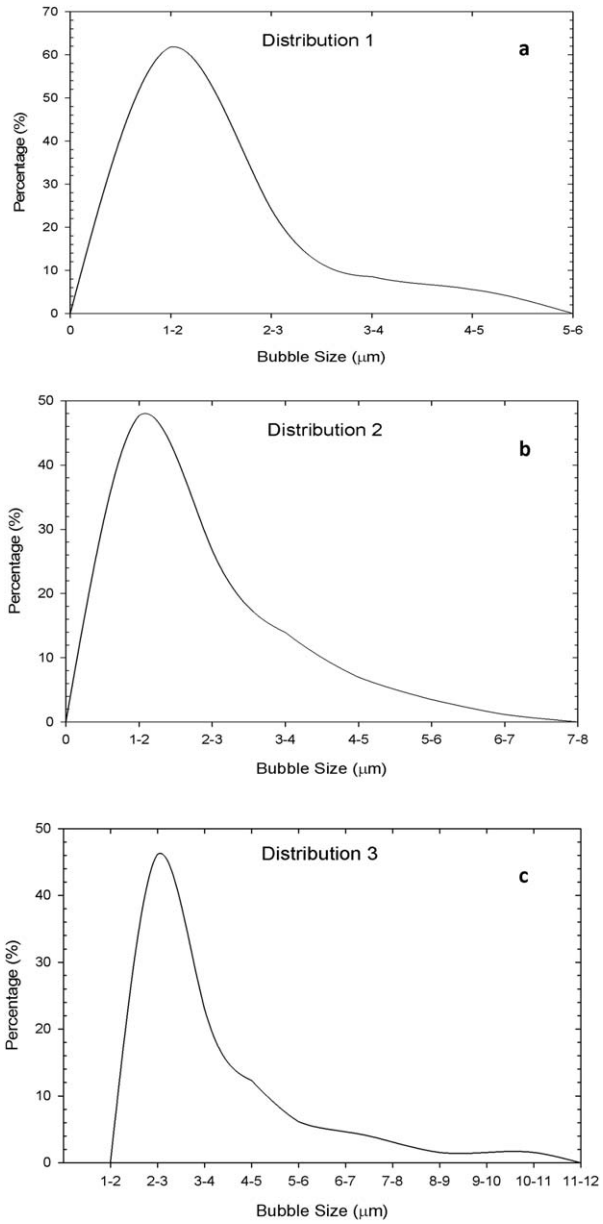

Figure 5. Bubble size distributions (a) Distribution 1, (b) Distribution 2, and (c) Distribution 3.

To have a better understanding of microbubble deformation through capillary tube differential pressure measurements, the capillary number was measured $\left(\mathrm{Ca}=\frac{\mu_c \gamma a}{\sigma}\right)$. In this study, Ca was varied from 4.6×10^{-6} to 3.8×10^{-4} depending on the bubble size distribution. As mentioned by Pal[29] for small values of Ca, close to zero ($\mathrm{Ca} < 0.01$), microbubbles can be assumed to be undeformable. Therefore, in this study, due to Ca numbers close to zero, microbubbles are assumed to be undeformable.

Rheology of Microbubbles

In this work, the theoretical expression given by Rabinowitsch[30] was used to calculate the rate of the shear to microbubbles. This theoretical analysis was also presented by Mooney[31] and Metzner and Reed[32]. It has also been applied to measure viscosities of liquid–liquid emulsions by Alvarado and Marsden.[33] The expressions are as follows

$$\tau_w = \frac{R\Delta P}{2L} \tag{1}$$

$$\tau_w = K'\left(\frac{8V}{D}\right)^{n'} \tag{2}$$

$$\dot{\gamma}_w = \frac{3n'+1}{4n'}\left(\frac{8V}{D}\right) \tag{3}$$

where τ_w and $\dot{\gamma}_w$ are shear stress and shear rate at the capillary wall, respectively. Capillary radius, diameter, and length are denoted by R, D, and L. ΔP is the pressure drop along the capillary tube and V is the average flow velocity. Equation 1 is used to calculate wall shear stress. As Eqs. 1 and 2 are both expressing wall shear stress, one can write

$$\frac{R\Delta P}{2L} = K'\left(\frac{8V}{D}\right)^{n'} \tag{4}$$

The value of $8V/D$ can be denoted as apparent shear rate. Therefore, we can write

$$\dot{\gamma}_a = \frac{8V}{D} \tag{5}$$

Apparent shear rate and the wall shear rate are related as

$$\dot{\gamma}_w = \frac{3n'+1}{4n'}\dot{\gamma}_a \tag{6}$$

According to Eq. 4, n' is the slope of the line drawn to represent $R\Delta P/2L$ vs. $8V/D$ on a logarithmic plot. Thus, n' can be calculated as follows

$$n' = \frac{d\ln\left(\frac{R\Delta P}{2L}\right)}{d\ln\left(\frac{8V}{D}\right)} \tag{7}$$

After obtaining n', K' can be found as the y-intercept of the line drawn representing $R\Delta P/2L$ vs. $8V/D$ on a logarithmic plot. It has been shown that K' and n' are constant over a wide range of shear stress and apparent shear rate for non-Newtonian fluids.[32]

By definition, apparent viscosity is known as

$$\mu_a = \frac{\tau_w}{\gamma_w} \tag{8}$$

Substituting Eqs. 2 and 3 into Eq. 8 results in the following equation, which is used to calculate the apparent viscosity of microbubble suspensions

$$\mu_a = \frac{4n'}{3n'+1}K'\left(\frac{8V}{D}\right)^{n'-1} \tag{9}$$

If wall shear rate is changed to apparent shear rate in Eq. 8, the apparent viscosity will be effective viscosity. The effective viscosity is accordingly defined as

$$\mu_e = K'\left(\frac{8V}{D}\right)^{n'-1} \tag{10}$$

The apparent viscosity calculated from Eq. 10 is the experimental viscosity of microbubbles obtained in this study from the pressure drop in capillary tubes.

In this study, the model proposed to predict the viscosity of microbubble suspensions in capillary tubes is started from Poiseuille's formula[34]:

$$\frac{\Delta P}{\rho_c V^2} = \frac{16}{Re_c}\left(\frac{L}{R}\right) \tag{11}$$

where ρ_c is the continuous phase density. Poiseuille's formula has been defined for fully developed laminar flow with a parabolic velocity profile. It has been suggested that the pressure drop in capillary tubes for single phase liquids is higher than the value predicted by Poiseuille's formula.[34] There are two main reasons for this difference in the pressure drop of a single phase flow in capillary tubes and the predicted value of Poiseuille's formula. First, in the initial part of the flow, the profile is changing from a near-uniform distribution to a parabolic velocity distribution. This will cause an additional pressure drop compared to Poiseuille's formula. Second, the acceleration at the center of the tube in the initial region of the flow causes a radial velocity which leads to a radial pressure drop. This additional pressure drop will result in an underestimation of Poiseuille's formula. Several investigators have tried to solve the underestimation of Poiseuille's formula, analytically, by simplified mathematics.[35,36]

Langhaar[35] proposed a modified equation for $Re_c \to \infty$. This equation was achieved by linearizing Navier–Stokes equations. The proposed equation is as follows

$$\frac{\Delta P}{\rho_c V^2} = \frac{16}{Re_c}\left(\frac{L}{R}\right) + 2m \tag{12}$$

where m is experimentally determined. Other investigators have applied numerical solutions to solve the problem.[37–41] All of the solutions present m in Eq. 12 as a function of Re_c. Therefore, Eq. 12 can be written as

$$\frac{\Delta P}{\rho_c V^2} = \frac{16}{Re_c}\left(\frac{L}{R}\right) + m(Re_c) \tag{13}$$

Kestin et al.[34] provided a correlation for m. Their study was done for $0.5 < Re_c < 100$. They concluded that their correlation could also be applied to $Re_c > 100$, as the values of their correlation in Re_c exceeding 100 were close to values presented by Langhaar.[35] They correlated m as

$$m = m_0 + \frac{8n}{Re_c} \tag{14}$$

m_0 and n are constants, which need to be found experimentally. To reach the viscosity, they introduced the proposed equation (Eq. 14) into Eq. 13, which resulted in

$$\mu_a = \frac{\pi R^4 \rho_c}{8(L+nR)} \left(\frac{\Delta P}{\dot{m}} - \frac{m_0 \dot{m}}{\rho_c \pi^2 R^4} \right) \quad (15)$$

Equation 15 uses a virtual length instead of the actual tube length. The virtual length $(L' = L + nR)$ corrects Poiseuille's formula, creating a better prediction of capillary tube pressure drop and viscosity. In their study, m_0 and n were found, theoretically, to be 1.17 and 0.69, respectively.

It has been found by Kestin et al.[34] that the behavior of fluids in capillary tubes is sensitive to the inlet conditions. The inlet conditions include both the shape of the tube at the entrance and the size of the injection reservoir, compared to the capillary diameter. In this study, in order to eliminate the effect of the injection reservoir size, the plexiglass chambers used to inject microbubbles into the tube were chosen to be considerably larger than the tube diameter. Furthermore, capillary tubes were square-cut at the entrance, so as to have a sharp inlet for the flow.

In this study, Eq. 15 was tried to predict the viscosity of microbubble suspensions. It was found that Eq. 15 was capable of predicting microbubble viscosities in a constant bubble void fraction by changing the coefficients (m_0 and n). However, when the bubble fraction was changed, Eq. 15 was unable to predict microbubble viscosities. Therefore, L' was modified in order to obtain a better prediction. In this study, L', which was defined as $L + nR$ in Eq. 15, was modified for different bubble void fractions as follows

$$L' = (L+nR)\left(\frac{\phi}{\phi_r}\right)^x \quad (16)$$

where x is a constant that is found experimentally and ϕ_r is the reference gas void fraction, which is the bubble percentage in which m_0 and n are determined. Thus, Eq. 15 was modified to

$$\mu_a = \frac{\pi R^4 \rho_c}{8(L+nR)\left(\frac{\phi}{\phi_r}\right)^x} \left(\frac{\Delta P}{\dot{m}} - \frac{m_0 \dot{m}}{\rho_c \pi^2 R^4} \right) \quad (17)$$

Parameters m_0, n, and x need to be found through an optimization process. To find these parameters, the data from a constant bubble fraction (ϕ_r) were used to reach the parameters in Eq. 15 (m_0 and n). After obtaining m_0 and n, the data from different gas void fractions were applied to Eq. 17 in order to reach x. To perform optimization, half of the data was selected randomly. After finding the parameters, the other half of the data was used to verify the model with the fitting parameters.

In the introduced correlation (Eq. 17), viscosities of microbubbles can be predicted using their bubble void fraction. As mentioned before, although the value of viscosity changes with tube conditions, the rheological behavior of microbubbles is dependent on the bubble void fraction. In other words, n' only depends on bubble void fraction. Therefore, in Eq. 9, which is used to calculate experimental viscosity, the effect of bubble void fraction is presented by n'. To accomodate the effect of the bubble void fraction on their apparent viscosity in the proposed equation (Eq. 17), the modification introduced in Eq. 16 $\left(\left(\frac{\phi}{\phi_r}\right)^x\right)$ was implemented.

Results and Discussion

The calculated n' from Eq. 7 represents the flow behavior index, which demonstrates the rheological behavior of microbubbles. In Figures 6–8, μ_a vs. $8V/D$ are shown in *Ln-Ln* plots. Figures 6 and 7 show the plots of different tube diameters and lengths, respectively. Figure 8 presents the lines of different bubble void fractions. According to Eq. 9,

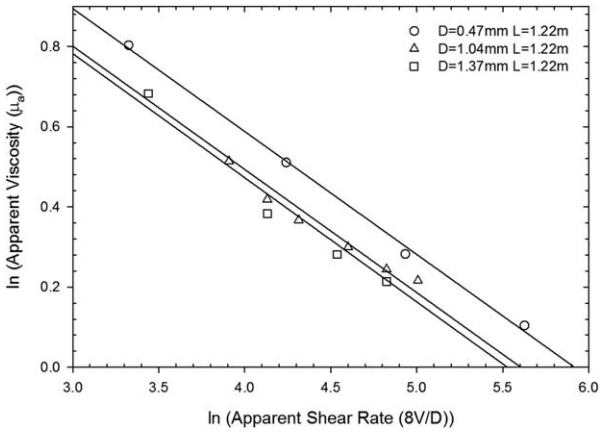

Figure 6. Apparent viscosity vs. apparent shear rate for different tube diameters, constant tube length, and constant bubble void fraction (ϕ = 4.9%).

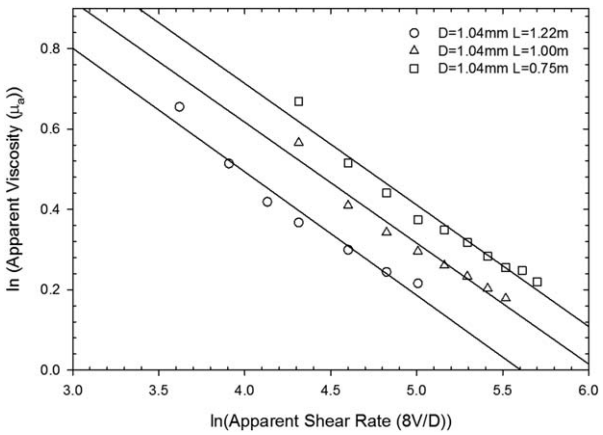

Figure 7. Apparent viscosity vs. apparent shear rate for different tube length, constant tube diameter, and constant bubble void fraction (ϕ = 4.9%).

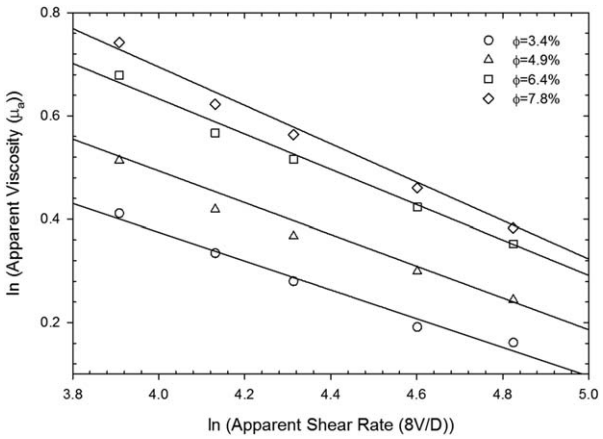

Figure 8. Apparent viscosity vs. apparent shear rate for different bubble void fractions, constant tube diameter and length (D = 1.04 mm and L = 1.22 m).

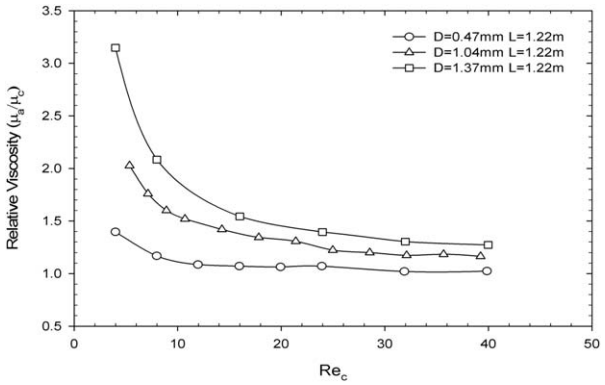

Figure 9. Experimental data results for microbubble viscosity in different tube diameters and constant tube lengths and void fraction ($\phi = 4.9\%$).

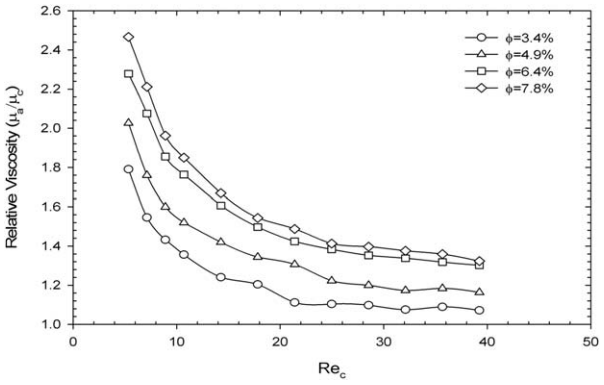

Figure 11. Experimental data results for microbubble viscosity in different bubble void fractions and constant tube diameters and lengths ($D = 1.04$ mm and $L = 1.22$ m).

the slopes of the lines show $(n' - 1)$ for each series of data. Therefore, lines with the same slopes are representing suspensions with similar rheological behavior. The higher the absolute value of the slopes of the lines is from zero, the more the suspensions deviate from Newtonian behavior.

In Figures 6 and 7, although the value of the viscosity changes for different tube diameters and lengths, the slopes of the lines are constant (−0.30). This is due to a constant bubble void fraction in suspensions. However, in Figure 8, the slope of the line changes for different bubble void fractions (−0.27 to −0.37). This suggests that tube conditions may affect viscosity, but the rheological behavior is determined by the percentage of bubbles in the suspension.

The results for the relative viscosities of microbubbles in different tube diameters and lengths are shown in Figures 9 and 10. Moreover, the results for different bubble void fractions can be found in Figure 11.

Figures 9–11 illustrate the relationship of viscosity and Re_c. When Re_c increases, the viscosity of microbubbles decreases. The viscosity decreases until it reaches a constant value. Increasing Re_c after this point results in a constant viscosity of microbubbles. This represents the non-Newtonian behavior of microbubbles in the capillary tubes. It is known[12,13] that small bubbles (<0.6 mm) start to concentrate close to the tube walls upon their entrance into a tube. This causes the void profile of the gas to demonstrate two maximas close to the tube walls and a constant value at the center of the tube. By increasing Re_c, the bubble distribution becomes more uniform in the center of the tube and the two maximums close to walls start to diminish. As mentioned by Valukina et al.[12] for increased values of Re_c, the friction factor in tubes is decreased. A decrease in the friction factor leads to a lower viscosity of the suspension and a lower pressure drop across the tube. In Figure 9, a decrease in viscosity with the decrease in tube diameters is observed. This was also caused by a different bubble orientation on the cross section of the tube. Smaller tube diameters lead to more uniform void distributions in a constant bubble concentration, which causes less pressure drop across the tube and smaller viscosity values.

Figure 10 represents the effect of tube length on the viscosity of microbubbles. Smaller viscosities are observed in longer tubes. According to Kestin et al.[34] in capillary tube viscometry, there is an additional pressure drop caused by the developing region at the beginning of the flow. In this work, the effect on the viscosity of microbubbles was more pronounced than in single phase flow. The pronounced effect was caused by the disturbance of the developing region of bubble distribution, which was present in addition to the velocity profile developing region of the continuous phase. As the length of the tube increased, the additional pressure drop caused by the developing regions got smaller, compared

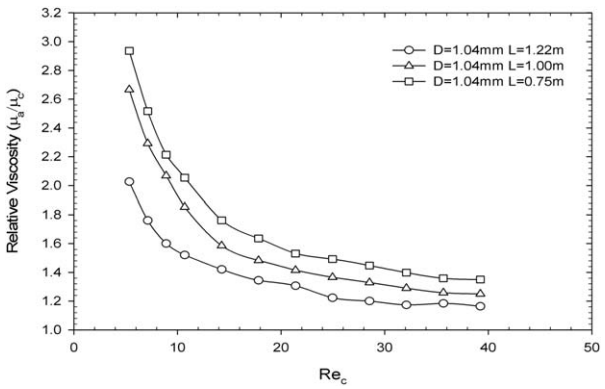

Figure 10. Experimental data results for microbubble viscosity in different tube lengths and constant tube diameters and void fraction ($\phi = 4.9\%$).

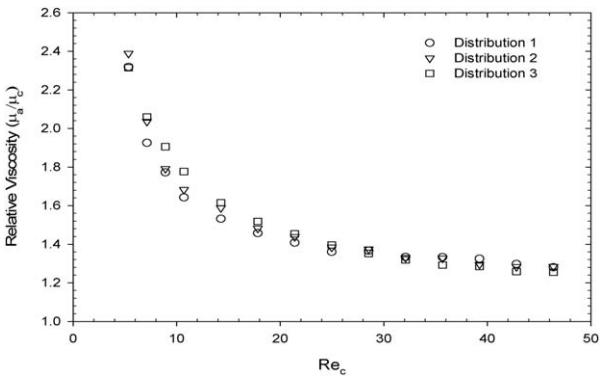

Figure 12. Experimental results for microbubble viscosity in different bubble size distributions with a constant bubble void fraction (Tube: $D = 1.04$ mm, $L = 1.22$ m, and $\phi = 6.4\%$).

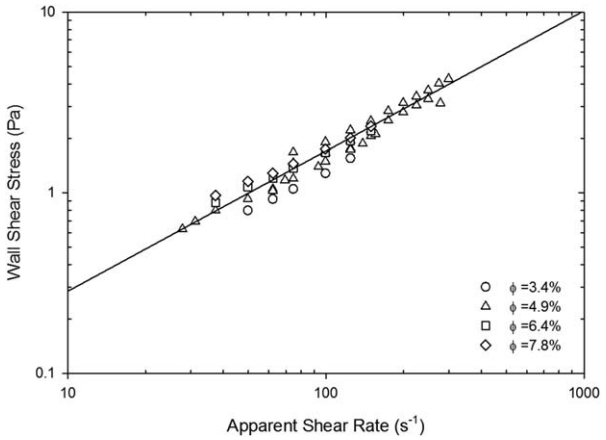

Figure 13. Wall shear stress vs. apparent shear rate for different bubble void fractions and different tube conditions at 4.9% bubble void fraction.

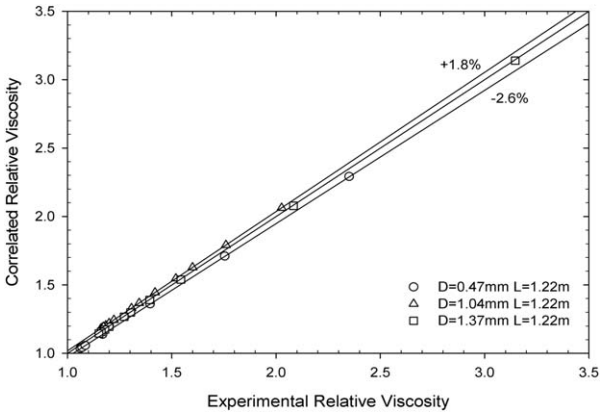

Figure 14. Experimental data vs. proposed correlation results for different tube diameters at a constant tube length and bubble void fraction (ϕ = 4.9%).

to the overall pressure drop. Thus, the calculated viscosity decreased as the tube length increased.

Figure 11 illustrates the effect of bubble void fraction on the viscosity of suspensions. As the fraction of the bubbles increased the viscosity increased. It has been reported that an increase in bubble void fraction increases the wall friction factor.[16] An increase in friction factor results in the increase of viscosity, which eventually leads to the increase in pressure drop of suspensions in capillary tubes.

Beside the bubble void fraction, the effect of bubble size distribution on the viscosity of the suspension was taken into consideration. To study the effect of size distribution, the viscosities of suspensions were measured in different bubble size distributions while keeping the quality of the suspensions constant. The pictures of suspensions and bubble size distributions have been shown in Figures 4 and 5.

The viscosities of different bubble size distributions have been measured in identical tubes to eliminate all of the affecting parameters except bubble size distribution. The viscosity results are shown in Figure 12. The results illustrate similar viscosity values for different bubble size distributions in constant Re_c numbers. This represents the independency of suspensions' viscosities from bubble size distribution. As previously reported by Chernyshev,[16] it is expected to have independency of suspensions' flow behavior from bubble size distribution in small bubble size ranges (<0.5 mm). The results in this study confirm the finding previously reported by Chernyshev.[16]

Power law has been applied to represent non-Newtonian behavior of microbubbles.[17] In this study, power law's capability in explaining apparent viscosity of microbubbles in capillary tubes has been evaluated. Power law relates wall shear stress and apparent shear rate as Eq. 2. In other words, one can write

$$\tau_w = K' \dot{\gamma}_a^{\,n'} \tag{18}$$

The apparent viscosity from power law is calculated as

$$\mu_a = \frac{4n'}{3n'+1} K' \dot{\gamma}_a^{\,n'-1} \tag{19}$$

The ability of Eq. 19 in predicting apparent viscosity depends on its success in having the best regressed n' and K' for different conditions to relate wall shear stress and apparent shear rate. Figure 13 represents microbubbles' wall shear stress vs. apparent shear rate in a log–log plot.

The linear line drawn in Figure 13 presents the power law relation between wall shear stress and apparent shear rate based on the best regressed values of n' and K' in Eq. 18 as follows

$$\tau_w = 0.049 \dot{\gamma}_a^{\,0.76} \tag{20}$$

Consequently, the apparent viscosity is

$$\mu_a = 0.046 \dot{\gamma}_a^{\,0.24} \tag{21}$$

It is found that the absolute average relative deviation (AARD) of the data from the proposed power law equation is 16.1%. Thus, it is concluded that power law is not capable of predicting microbubbles' behavior in capillary tubes under different conditions. The deficiency of power law in predicting microbubbles' behavior is mainly related to the change in rheological properties of microbubbles of different void fractions. Therefore, it is essential to have an equation that can predict microbubbles' viscosity in different conditions, especially different bubble void fractions.

Equation 17 was used to obtain the experimental relative viscosity data. In this work, m_0, n, and x were found to be equal to 1.25, 207.1, and 0.024, respectively. Compared to single phase studies performed by previous investigators, m_0

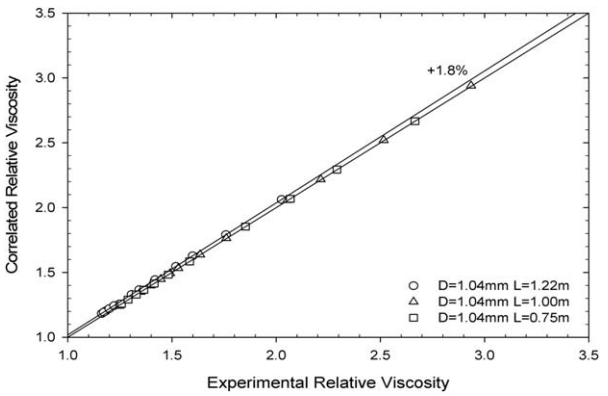

Figure 15. Experimental data vs. proposed correlation results for different tube lengths at a constant tube diameter and bubble void fraction (ϕ = 4.9%).

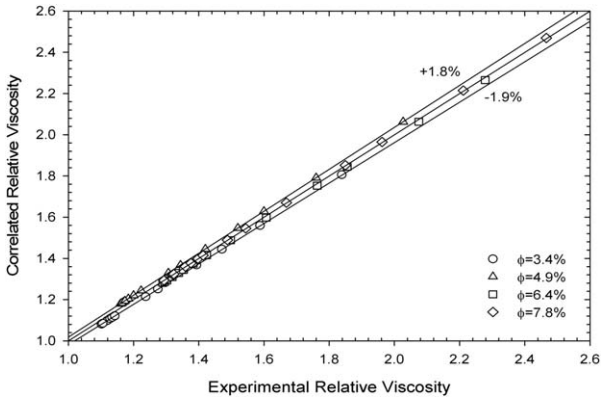

Figure 16. Experimental data vs. proposed correlation results for different bubble void fractions at a constant tube diameter and length ($D = 1.04$ mm and $L = 1.22$ m).

is in the same order. However, n, which defines the virtual length, has increased considerably. This is due to the presence of microbubbles, which causes a higher pressure drop as compared to a single phase fluid. This has caused the virtual length to be higher than in single phase studies in order to represent the extra pressure drop.

Figures 14–16 show the comparison between the experimental relative viscosity and the relative viscosity results from the proposed correlation. The reason for using relative viscosity in comparing the experimental and correlated results is to see the effect of bubbles on the viscosity of the suspension. In other words, the ability of the correlation in predicting the bubble effects on suspension's viscosity is shown in Figures 14–16; this illustrates that the proposed correlation is capable of predicting the relative viscosity of microbubbles in tubes of different diameters (Figure 14: $D = 0.47$, 1.04, and 1.37 mm, $L = 1.22$ m, $\phi = 4.9\%$) and different lengths (Figure 15: $L = 0.75$, 1.00, and 1.22 m, $D = 1.04$ mm, $\phi = 4.9\%$) and different bubble void fractions (Figure 16: $\phi = 3.4$, 4.9, 6.4, and 7.8%) in the range of $Re_c < 50$, with AARD under 1.3%. The maximum deviation between the experimental data and the proposed correlation results was equal to 2.6%.

Conclusions

In this study, experiments were conducted to determine microbubble viscosity in capillary tubes. The viscosity of microbubbles was measured in three different tube sizes and lengths. Moreover, viscosities in different bubble void fractions and with different bubble size distributions were investigated.

The microbubbles presented non-Newtonian behavior. When Re_c was increased, the viscosity of microbubbles decreased. The viscosity decreased until it reached a constant value. Increasing Re_c after this point resulted in a constant viscosity of microbubbles.

The viscosity of microbubbles decreased as the tube diameter decreased and the tube length increased. This reduction in viscosity was due to different bubble orientations in the cross section of the tube. Furthermore, the viscosities of the suspensions increased with an increase in the bubble void fraction. The increase in viscosity because of an increase in the void fraction of bubbles coincides with a change in the flow behavior index (n'). However, the change in the viscosities of microbubbles due to a change in capillary tube length and diameter did not affect the flow behavior index. These results showed that although tube conditions change viscosity values, they do not affect the rheological behavior of suspensions. The only parameter that affects the flow behavior index is the void fraction of bubbles. The effect of bubble size distribution was also investigated. It was found that, in the bubble size range of 1–12 μm, the size distribution of bubbles did not influence the viscosity of suspensions.

It was found that the power law was unable to predict the microbubbles' behavior in capillary tubes with different bubble void fractions. Therefore, data obtained from experiments were used to develop a correlation to predict the viscosity of microbubbles flowing through capillary tubes. A good agreement between experimental viscosity data and correlated results was obtained. The developed correlation is capable of predicting microbubble viscosity in the range of $Re_c < 50$.

Acknowledgments

The authors acknowledge with thanks the financial support from Discovery Grant of Natural Sciences and Engineering Research Counsel (NSERC) of Canada and The Natural Science Foundation of China (Project No: 51274225).

Notation

AARD = absolute average relative deviation
a = bubble radius, μm
Ca = capillary number, dimensionless
D = capillary diameter, cm
K' = consistency constant, poise $s^{1-n'}$
L = capillary length, m
m = constant
m_0 = constant
$\dot{m}$ = mass flow rate, g/s
n = constant, dimensionless
n' = flow index, dimensionless
R = capillary radius, cm
Re_c = continuous phase reynolds number, dimensionless
V = average fluid velocity, cm/s
x = constant, dimensionless
ΔP = pressure drop along the capillary tube, Pa
ρ_c = continuous phase density, g/cm^3
μ_a = apparent viscosity, Pa s
μ_c = continuous phase viscosity, Pa s
μ_e = effective viscosity, Pa s
μ_r (μ_a/μ_c) = relative viscosity, dimensionless
ϕ = bubble void fraction, dimensionless
ϕ_r = reference bubble void fraction, dimensionless
σ = interfacial tension, mN/m
τ_w = wall shear stress, Pa
$\dot{\gamma}_w$ = wall shear rate, s^{-1}
$\dot{\gamma}_a$ = apparent shear rate, s^{-1}

Literature Cited

1. Sebba F. Microfoams-an unexploited colloid system. *Colloid Interface Sci*. 1971;35:643–646.
2. Sebba F. Foams and Biliquid Foams-Aphrons. New York: Wiley, 1987:46–61, 62–78, 102–127.
3. Cassell EA, Kaufman KM, Matuevic E. The effects of bubble size on microflotation. *Water Res*. 1975;9:1017–1024.
4. Pitt WG, Husseini GA, Staples BJ. Ultrasonic drug delivery—a general review. *Expert Opin Drug Deliv*. 2004;357:37–56.
5. Ivan CD, Quintana JL, Blake LD. Aphron-base drilling fluid: evolving technologies for lost circulation control. *SPE Annual Technical Conference and Exhibition*. New Orleans, LA, September 30 to October 3, 2001.

6. Samuel SR, Kuru E, Trivedi JJ. Design and development of aqueous colloidal gas aphrons for enhanced oil recovery applications. *SPE Improved Oil Recovery Symposium*. Tulsa, OK, 2012.
7. Wang S, Clarens AF. The effects of CO_2-brine rheology on leakage processes in geologic carbon sequestration. *Water Resour Res*. 2012; 48:W08518.
8. Xue Z, Yamada T, Matsuoka T, Hiromichi Kameyama H, Nishio S. Carbon dioxide microbubble injection-Enhanced dissolution in geological sequestration. *Energy Procedia*. 2011;4:4307–4313.
9. Sheikha H, Pooladi-Darvish M. Micro bubbles in solution-gas drive in heavy oil: their existence and importance. *Transp Porous Media*. 2012;93:495–516.
10. Kashinsky ON, Timkin LS, Cartellier A. Experimental study of "laminar" bubbly flows in a vertical pipe. *Exp Fluids*. 1993;15:308–314.
11. Burdukov AP, Koz'menko BK, Nakoryakov VE. Distribution of the velocity profiles of the liquid phase in a gas-liquid flow with small gas contents, *J Appl Mech Tech Phys*. 1975;16:862–864.
12. Valukina NV, Koz'menko BK, Kashinskii ON. Characteristics of a flow of monodisperse gas-liquid mixture in a vertical tube. *J Eng Phys*. 1979;36:462–465.
13. Nakoryakov VE, Kashinskii ON, Shevchenko VI. Local gas content and velocity of the liquid phase in ascending bubble flow. *J Eng Phys*. 1987;52:125–129.
14. Burdukov AP, Valukina NV, Nakoryakov VE. Special characteristics of the flow of a gas-liquid bubble-type mixture with small reynolds numbers. *J Appl Mech Tech Phys*. 1975;16:592–596.
15. Kashinskii ON, Krokovnyi PM. Experimental investigation of velocity profiles in a horizontal gas-liquid stream. *J Appl Mech Tech Phys*. 1979;20:449–452.
16. Chernyshev IV. Microbubble medium: production and hydrodynamic properties. *J Atom Spr*. 1997;6:649–661.
17. Tseng H, Pilon L, Warrier GR. Rheology and convective heat transfer of colloidal gas aphrons in horizontal mini-channels. *Int J Heat Fluid Flow*. 2006;27:298–310.
18. Grinstaff MW, Suslick KS. Air-filled proteinaceous microbubbles: synthesis of an echo-contrast agent. *Proc Natl Acad Sci USA*. 1991; 88:7708–7710.
19. Zhou M, Cavalieri F, Ashokkumar M. Modification of the size distribution of lysozyme microbubbles using a post-sonication technique. *Instrum Sci Technol*. 2012;1:51–60.
20. Farook U, Stride E, Edirisinghe MJ, Moaleji R. Microbubbling by co-axial electrohydrodynamic atomization. *Med Biol Eng Comput*. 2007;45:781–789.
21. Garstecki P, Fuerstman MJ, Stonec HA, Whitesides GM. Formation of droplets and bubbles in a microfluidic T-junction-scaling and mechanism of break-up. *Lab Chip*. 2006;6:437–446.
22. Yasuno M, Sugiura S, Iwamoto S, Nakajima M. Monodispersed microbubble formation using microchannel technique. *AIChE J*. 2004;50:3227–3233.
23. Xu JH, Li SW, Chen GG, Luo GS. Formation of monodisperse microbubbles in a microfluidic device. *AIChE J*. 2006;52:2254–2259.
24. Sebba F. An improved generator for micron-sized bubbles. *Chem Ind*. 1985;4:91–92.
25. Wan J, Veerapaneni S, Gadelle F, Tokunaga TK. Generation of stable microbubbles and their transport through porous media. *Water Resour Res*. 2001;37:1173–1182.
26. Save SV, Pangarkar VG. Characterization of colloidal gas aphrons. *Chem Eng Commun*. 1994;127:35–54.
27. Wheatley MA, Shen P, Singhal S, Goldberg BB. Surfactant stabilized microbubble mixtures process for preparing and methods of using the same. Patent 5,352,436. U.S. Patent Office: Washington DC, 1994.
28. Cervantes-Martínez A, Saint-Jalmes A, Maldonado A, Langevin D. Effect of cosurfactant on the free-drainage regime of aqueous foams. *J Colloid Interface Sci*. 2005;292:544–547.
29. Pal R. Rheology of Particulate Dispersions and Composites. Surface Science Series, Vol. 136. Boca Raton, FL: CRC Press, 2010.
30. Rabinowitsch B. Viscosity and elasticity of sols. *Z Phys Chem*. 1929;AM3:1–29.
31. Mooney M. Explicit formulas for slip and fluidity. *J Rheol*. 1931;2: 210–223.
32. Metzner AB, Reed JC. Flow of non-newtonian fluids-correlation of the laminar, transition, and turbulent-Flow Regions. *AIChE J*. 1955; 1:434–440.
33. Alvarado DA, Marsden SS Jr. Flow of oil-in-water emulsions through tubes and porous media. *SPE J*. 1979;19:369–377.
34. Kestin J, Sokolov M, Wakeham W. Theory of capillary viscometers. *Appl Sci Res*. 1973;27:241–264.
35. Langhaar HL. Steady flow in the transition length of a straight tube. *J Appl Mech*. 1942;64:A55–A58.
36. Sparrow EM, Lin SH, Lundgren TS. Flow development in the hydrodynamic entrance region of tubes and ducts. *Phys Fluids*. 1964;7:338–347.
37. Christiansen EB, Lemmon HE. Entrance region flow. *AIChE J*. 1965;11:995–999.
38. Schmidt FW, Zeldin B. Laminar flows in inlet sections of tubes and ducts. *AIChE J*. 1969;15:612–614.
39. Hornbeck RW. Laminar flow in the entrance region of a pipe. *Appl Sci Res*. 1964;A13:224–232.
40. Vrentas JS, Duda JL, Bargeron KG. Effect of axial diffusion of vorticity on flow development in circular conduits: part I. *Numerical solutions. AIChE J*. 1966;12:837–844.
41. Friedman M, Gillis J, Liron N. Laminar flow in a pipe at low and moderate reynolds numbers. *Appl Sci Res*. 1968;19:426–438.

Manuscript received Oct. 3, 2013, revision received Jan. 3, 2014, and final revision received Mar. 4, 2014.